Supplement of Solid Earth, 14, 293–310, 2023
https://doi.org/10.5194/se-14-293-2023-supplement

Solid Earth Open Access EGU

Supplement of

Transport mechanisms of hydrothermal convection in faulted tight sandstones

Guoqiang Yan et al.

Correspondence to: Guoqiang Yan (guoqiang.yan@kit.edu)

The presented model on the scale of faulted hydrothermal systems is validated against the results of the study conducted by Malkovsky and Magri (2016) and Guillou-Frottier et al. (2020). An identical geometry, fluid and rock properties, initial conditions, and boundary conditions, e.g., a 40 m wide and 10^{13} m^2 permeable fault zone embedded in impervious host rock (cube of 5.5 km), heat conductivity of rock of 2 W m^{-1} K^{-1}, the fixed top temperature of 20 °C and bottom temperature of 170 °C of the domain are assumed here. It needs to be mentioned that different from the fluid density and dynamic viscosity shown in equations (4) and (5), the fluid density varies linearly with temperature over the 0 ~ 150 °C range. The fluid density is given as

$$\rho^l = 1022.38 \cdot [1 - 5.9 \cdot 10^{-4} \cdot (T - 293.15)] \quad \text{(S1)}$$

where ρ^l is the fluid density (kg·m^{-3}) and T is the temperature (K). The dynamic viscosity is written as

$$\mu = 1.17 \cdot 10^{-3} \cdot \left(\frac{293.15 - T}{62.1}\right) \quad \text{(S2)}$$

where μ is the fluid dynamic fluid viscosity (Pa s).

The transient evolution of our model is computed from 0 s to 10^{13} s. Our model reproduces the results including displaying the onset and long-term characteristics of buoyancy-driven convection in the fault plane (Fig. S1). At $t = 10^{13}$ s, the buoyancy-driven convection in the main fault results in three convective cells which consist of two downflows and upflows in each (Fig. S1a). The mentioned upward and downward flows of fluids generate one full and one-half thermal plumes, as shown in Fig. S1b. The temperature distribution in the host rock is mainly dominated by heat conduction, as shown in Fig. S1a. Affected by the upward flows above the -4 km location and downward flows below the -4 km location, the central line of the model shows positive and negative thermal anomalies compared to the initial temperature distribution, respectively.

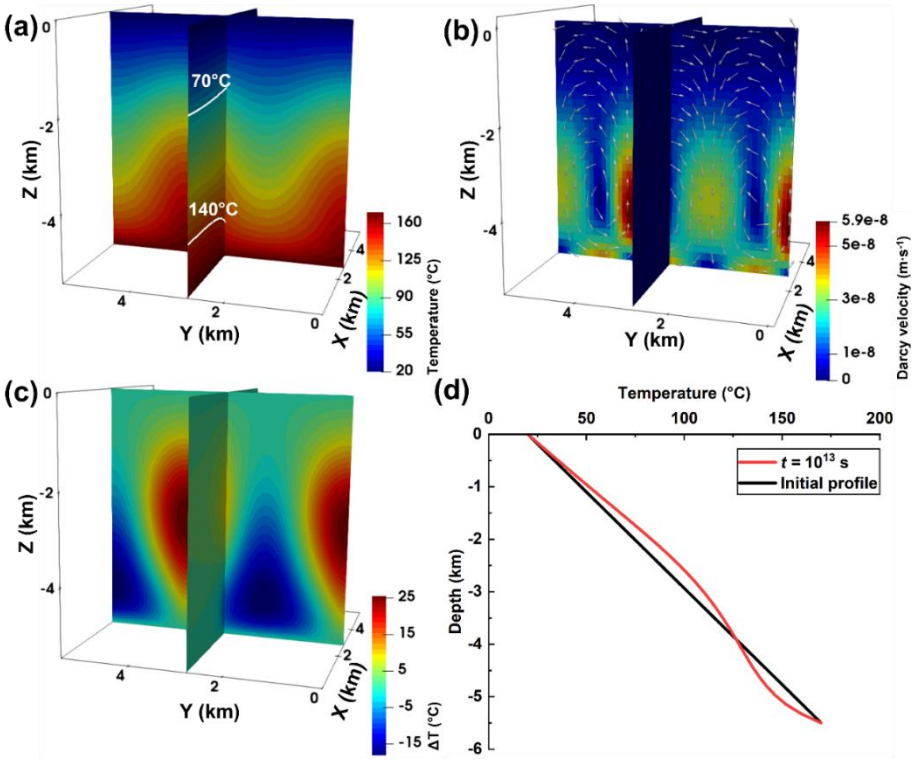

Figure S1. Fluid flow and temperature fields of a 40 m wide fault zone embedded in impervious host rock (cube of 5.5 km). At $t = 10^{13}$ s, cross-sectional views of the (a) resulting temperature distributions. The 70 °C and 140 °C isotherms are highlighted to indicate the dominant heat transfer types; (b) flow field with arrows representing the preferential fluid flow pathways; (c) temperature differences compared to the initial conductive temperature distribution. (d) Temperature-depth profiles that follow the central line of the model at the initial time and $t = 10^{13}$ s, respectively.

Table S1. Temperature perturbations at $t = 10^{13}$ s compared to initial time in different simulators.

Simulator	Temperature perturbation range (°C)	Contributor
Tiger	-18.2 ~ +25.4	our model
OpenGeoSys	-20.62 ~ +28.94	Malkovsky and Magri (2016)
Comsol Multiphysics™	-21.7 ~ +32.1	Guillou-Frottier et al. (2020)

The patterns of buoyancy-driven convection in the fault plane are qualitatively similar to the results (i.e., same convective cells number and locations) of the other two simulators. Meanwhile, differences in the temperature perturbations and maximum Darcy velocity magnitude can be observed in the details of the results. Compared to the initial temperature distribution, the buoyancy-driven convection results in the temperature perturbations have the range of -18.2 °C and +25.4 °C, lower than the results of OpenGeoSys and Comsol Multiphysics™ (Fig. S1c and Table S1). Fig. S1b illustrates that the maximum Darcy velocity is $5.9 \cdot 10^{-8}$ m·s^{-1}, which is lower than the maximum Darcy velocity of $7.3 \cdot 10^{-8}$ m·s^{-1} in (Guillou-Frottier et al. 2020) (shown in their Fig. B2(a)). As explained by Malkovsky and Magri (2016), numerical instabilities may easily develop in density-driven flow problems. In addition, the time discretization adopted by different applications may also differ from that imposed in the other numerical codes. Thus, our model on the scale of faulted hydrothermal systems has been successfully validated here, taking into account the acceptable differences described above.

Reference

Guillou-Frottier, Laurent; Duwiquet, Hugo; Launay, Gaëtan; Taillefer, Audrey; Roche, Vincent; Link, Gaétan (2020): On the morphology and amplitude of 2D and 3D thermal anomalies induced by buoyancy-driven flow within and around fault zones. In Solid Earth 11 (4), pp. 1571–1595. DOI: 10.5194/se-11-1571-2020.

Malkovsky, Victor I.; Magri, Fabien (2016): Thermal convection of temperature-dependent viscous fluids within three-dimensional faulted geothermal systems: Estimation from linear and numerical analyses. In Water Resour. Res. 52 (4), pp. 2855–2867. DOI: 10.1002/2015WR018001.